J Mater Sci (2023) 58:383–396

Materials for life sciences

Porous design of molecularly imprinted polymers for improved drug loading and organized release properties

Lan Luo[1], Chengkai Lv[1], Yukun Xing[1], Fen Ma[1], Jie Kong[2], and Fangfang Chen[1,*]

[1] *Key Laboratory of Synthetic and Natural Functional Molecule Chemistry of the Ministry of Education, College of Chemistry and Materials Science, Northwest University, Xi'an 710069, China*

[2] *Shaanxi Key Laboratory of Macromolecular Science and Technology, School of Chemistry and Chemical Engineering, Northwestern Polytechnical University, Xi'an 710072, China*

Received: 8 August 2022
Accepted: 1 December 2022
Published online: 13 December 2022

ABSTRACT

Molecular imprinting materials can successfully improve the efficacy and safety of drugs, thus showing good potential in the field of drug delivery. However, some difficulties in imprinted materials, such as the deep embedding of imprinting sites and poor accessibility, limit their application. Herein, we have developed porous designed molecularly imprinted polymers (MIPs) based on cleavage hyperbranched polymers for thiamine hydrochloride controlled release. By introducing hyperbranched polymers with terminal double bonds and sensitive disulfide bonds, the resulting porous MIPs (PMIPs) can expose more effective recognition sites and improve the drug-controlled release behavior, where significantly improved the drug loading (101.25 mg g^{-1}) compared with the porous non-imprinted polymers (PNIPs, 16.57 mg g^{-1}). Moreover, under the optimized conditions of pH 1.7 and 25 °C, the whole drug release time was increased from 16 h (PNIPs) to 32 h (PMIPs). As a result, this porous structure of MIPs designed approach provides an insight to fabricating improved imprinted constituents with higher adsorption capacity and faster recognition kinetics, which not only inspires more brilliant work in the future but also paves the way for the application of MIPs in the field of drug delivery.

Handling Editor: Annela M. Seddon.

Address correspondence to E-mail: chenff@nwu.edu.cn

https://doi.org/10.1007/s10853-022-08049-z

GRAPHICAL ABSTRACT

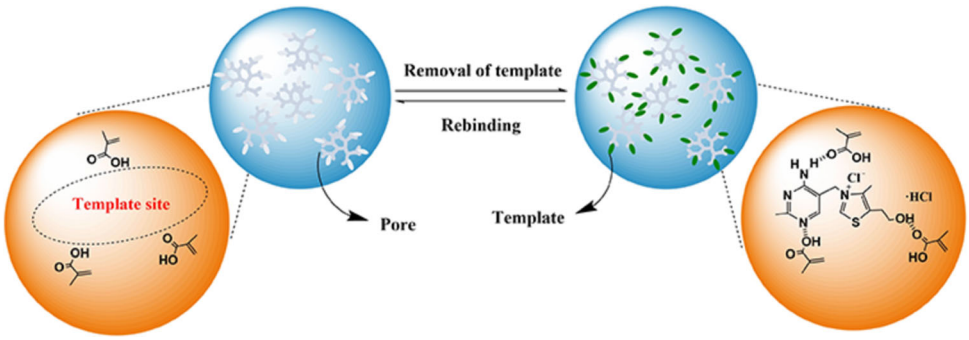

Introduction

In recent times, there has been augmented interest in controlled drug release systems based on nanomaterials because of their sustained release properties and large loading capacity [1–3]. Due to its unique advantage, controlled release nanomaterials can effectively overcome the problems caused by traditional drug administration, such as the concentration of drugs in vivo can only be maintained for a short time, resulting in the loss of efficacy [4, 5]. It not only prolongs the drug's duration but also makes its release smarter [6, 7]. Among the nanomaterials identified as carriers, molecularly imprinted polymers (MIPs) have predetermined selectivity of target molecules, attracting wide attention in developing drug delivery systems [8]. For instance, the redox-responsive molecularly imprinted nanoparticles based on biodegradable silica were designed to exhibit desirable targeted protein delivery and enhance tumor inhibition in cancer treatment [9].

MIPs is an artificial polymer with recognition sites complementary to target molecules [10], and the characteristics of controlled drug release triggered by imprinting sites of MIPs make them ideal for drug delivery research [11]. The interactions between template drug and imprinted sites are entirely different from that of traditional drug carrier models, such as physical adsorption or embedding, because of the affinity of the template to the functional monomer which is conducive to improving drug loading capacity and sustained release ability of MIPs [12]. With the development of molecular imprinting technology, there is wide applications of MIPs in fields such as sensing [13–15], chemical purification [16, 17], and delivery [18]. For instance, novel imprinted poly(methacrylic acid) nanoparticles for the controlled release of Rivastigmine Tartrate (RVs) were developed, which have the potential for RVS drug delivery to alleviate Alzheimer's and other diseases [19].

However, the MIPs prepared by conventional polymerization methods suffer from problems such as high crosslinking, the deep and tight embedding of imprinted sites, poor accessibility, and slow recognition kinetics, which affect the elution and resorption of template molecules, thus limiting the drug loading capacity of MIPs and its application in drug delivery systems [20]. To solve these problems and obtain better applicability, previous studies have revealed that MIPs with porous structures show superior advantages, which can expose the imprinted sites inside the materials; thus, faster recognition kinetics and higher adsorption capacity can be obtained [21]. We previously also reported porous MIPs with hyperbranched polymers for doxorubicin drug release [22]. The introduction of reversible covalent bonds into hyperbranched polymers can induce the cleavage and degradation of hyperbranched polymers under external stimulation, forming a porous MIPs structure that dramatically improves the recognition and sustained release properties of target molecules [23]. Hyperbranched polymers, with typical dendritic topology, have been found to have many unique properties, such as high

solubility, low chain entanglement, and numerous terminal functional groups [23–25]. Moreover, the easy functionalization promoted by these terminal groups on the backbone has attracted a lot of research activities [26]. Hence, introducing degradable hyperbranched polymers and MIPs in one reaction system is expected to be a reliable and feasible approach for preparing MIPs with porous structures to improve template drug loading and controlled release performance.

Thiamine hydrochloride (THC) is a vitamin B compound that may effectively prevent kidney disease in patients with type II diabetes [27]. THC deficiency can lead to conditions such as beriberi, resulting in fluid accumulation (swelling), pain, paralysis, and death. Vitamins from food are sometimes not entirely absorbed by the human body, so it is necessary to use a controlled drug release system to release it in the intestine [28]. In this contribution, porous designed MIPs have been developed based on hyperbranched polymers with sensitive cleavage bonds for THC controlled release. We designed and synthesized double bond-terminated hyperbranched polymers containing disulfide bonds via an $A_2 + B_3$ Michael addition method. The introduction of disulfide bonds into the hyperbranched polymers makes it easy to degrade and then be removed to form porous MIPs (PMIPs). Firstly, The A_2 monomer with sensitive disulfide and terminal double bond was synthesized as many active terminal functional groups reacted with cross-linked agents. Then, THC was selected as the template molecule, and the as-prepared double bond-terminated hyperbranched polymers were used as the matrix for preparing PMIPs. Due to the porosity and accessibility of recognition sites, the prepared PMIPs materials not only achieve the easily removal of template molecules, but also exhibited good adsorption performance and selectivity to template molecule THC versus other drugs. Finally, the PMIPs also possess sufficient drug loading capacity and responsive drug release, which proposes the benefits of using degradation hyperbranched polymers as a new matrix for designing the porous structure of MIPs to get the sustained release of drugs. The strategy of PMIPs provides a new idea for improving the effective utilization of imprinted sites and is also beneficial to the development of drug delivery systems.

Experiment section

Materials and reagents

Bis(2-hydroxyethyl) disulfide, *N*,*N*-dimethyl formamide (DMF), polystyrene (PS), 1-(2-aminoethyl)-piperazine (AP), and ethylene glycol dimethacrylate (EGDMA) were from Alfa Aesar Chemical Co., Ltd. (Tianjin China). Dithiothreitol (DTT), THC, theophylline, caffeine, indomethacin, and methyl acrylic acid (MAA) were from Aladdin Reagent Co., Ltd. (Shanghai, China). Acryloyl chloride, 2,2-azobisisobutyronitrile (AIBN), trimethylamine (TEA), and tetrahydrofuran (THF) were from J&K Scientific Ltd. (Beijing China). THF was used after strict water removal. Briefly, Added THF and sodium tablets in a two-row Schlenk device under the atmosphere of argon gas, which was then heated at 90 °C until the solvent changed from colorless to blue, where the chromogenic agent was diphenylketone.

Instrumentation

The infrared spectrum of the obtained materials was measured by a Nicolet IS10 Fourier transform infrared spectroscopy (FI-IR) spectrometer (Madison, USA). A Bruker Advance nuclear magnetic resonance (NMR) apparatus was applied to characterize the ^{1}H-NMR of A_2. The molecular weight and distribution of hyperbranched polymers were determined by a Waters 1515 gel permeation chromatography (GPC) apparatus (Massachusetts, USA). DMF and PS were used as a solvent and standard polymer, respectively. The elemental analysis was performed on a Thermo Fisher Scientific ESCALAB 250Xi X-ray photoelectron spectrometer (XPS, Waltham, USA) using a monochromatic Al K RX X-ray source. The external microstructure was observed on a ZEISS SUPRA 55 scanning electron microscope (SEM, Carl Zeiss Jena, German). Nitrogen sorption isothermal analysis was conducted on a Micromeritics Tristar II 3020 surface area analyzer (Georgia, USA). The data of ultraviolet–visible (UV) absorption were recorded on a Shimadzu UV-2250 spectrophotometer (Kyoto, Japan), and similar analytical procedures were previously reported by several works [29, 30].

Preparation of hyperbranched polymers

The esterification reaction synthesized bis(2-acryloxyethyl) disulfide ester with a double bond (A_2 monomer). The specific steps were as follows. Firstly, the Schlenk device was successively filled with argon gas, vacuumed, and heated so that no water or oxygen existed. Secondly, 7.3 g bis(2-hydroxyethyl) disulfide, 24.5 g TEA, and 200 mL anhydrous THF was added to the reaction flask was in an ice bath under an argon atmosphere. After adding the mixture of 17.7 g acryloyl chloride and 50 mL anhydrous THF drop by drop, the reaction occurred at room temperature for 24 h. Finally, the solvent was removed by vacuum distillation, and then the residue was dissolved in 100 mL methylene chloride. After successively washing with 100 mL NaCl solution and 100 mL deionized water three times, the appropriate amount of anhydrous Na_2SO_4 was added to the mixture which was then stirred for 30 min. Removed from the collected filtrate, which was further purified by silica gel chromatography and yielded orange viscous liquid as an A_2 monomer.

Hyperbranched polymer with disulfide linker and double bond terminals (HBP-AP) was then synthesized by the Michael addition method of "$A_2 + B_3$", where AP was selected as a B_3 monomer. Briefly, 0.576 g A_2 monomer (2.2 mmoL) and 260 μL B_3 monomer (1 mmoL) were added to 4 mL chloroform. After 24 h at 45 °C, the collected residuals were added to acetone twice to precipitate the polymer, and the yellow-colored viscous HBP-AP with cleavable disulfide linkers and alkene double bond terminals was collected by removing acetone by vacuum distillation.

Preparation of PMIPs

The PMIPs were prepared by precipitation polymerization using HBP-AP as a reaction substrate. The specific steps are as follows. 34 mg THC (template molecule) and 42 μL MAA were dissolved in the mixed solution of 9.6 mL acetonitrile and 2.4 mL water, stirring at room temperature for 3 h. Then, 100 mg HBP-AP, 480 μL EGDMA, and 30 mg AIBN were added to the pre-polymerization solution. After stirring for 20 min, the mixed solution was deoxygenated using argon for 15 min. The sealed flask was then placed in a thermostatic water bath for precipitation polymerization at 60 °C for 24 h. Subsequently, the solid particles in the reaction solution were collected by vacuum filtration, which was then extracted using a Soxhlet apparatus in methanol/water/acetic acid solution (6:3:1, $v/v/v$) until detected no THC in the solution. Afterward, the dried solid particles were added to 25 mL DTT (0.02 g mL^{-1}) and stirred to dissociate disulfide linkers from the cleavable HBP-AP in PMIPs. Finally, the obtained PMIPs were washed with water and dried at 60 °C.

In addition, non-imprinted polymers with HBP-AP (PNIPs) were prepared by the same procedure without THC. To be certain if improved the adsorption efficiency of the MIPs, MIPs and NIPs were designed without adding of HBP-AP as the reference, respectively.

Adsorption experiments

The adsorption properties of the obtained particles were characterized by static, dynamic, and selective adsorption experiments, where theophylline and caffeine were selected as analogs, and indomethacin was chosen as a reference compound. All tests were conducted thrice in parallel.

In the static adsorption experiments, 20 mg PMIPs, PNIPs, MIPs, or NIPs were dispersed in 3 mL THC solution with different initial concentrations (20–1200 mg L^{-1}), respectively. After stirring at 25 °C for 24 h, the supernatant was collected by centrifugation (4000 rpm), where the residual amount of THC was measured by a UV–vis spectrophotometer. The four adsorbents (20 mg for each) were evenly dispersed in 3 mL THC solution (40 mg L^{-1}) for the dynamic adsorption experiments. At the set stirring time (0–90 min), the residual amount of THC was measured by a UV–vis spectrophotometer. For the selective adsorption experiments, the four adsorbents (20 mg for each) were evenly dispersed in 3 mL THC, theophylline, caffeine, and indomethacin solution (40 mg L^{-1} for each), respectively. After stirring at 25 °C for 24 h, the residual amounts of the four compounds were measured by a UV–vis spectrophotometer respectively. Adsorption amount (Q, mg g^{-1}) was calculated by Eq. (1).

$$Q = (C_i - C_e)V/m \quad (1)$$

C_i (mg L^{-1}) and C_e (mg L^{-1}) are the initial and equilibrium concentrations of the testing solution, respectively. V (mL) is the volume of the solution. m (mg) is the mass of the adsorbent.

Study on influencing factors of drug loading

The influencing factors of drug loading were investigated, including the pH value of buffer, the mass of adsorbent, and adsorption temperature. THC was used as the model drug. Firstly, 20 mg PMIPs or MIPs was evenly dispersed in 3 mL THC solutions (40 mg L^{-1}) with different pHs ranging from 1.7 to 8.0. After stirring at 25 °C for 24 h, the residual amount of THC was measured by a UV–vis spectrophotometer, respectively. Secondly, different PMIPs or MIPs (5–30 mg) were evenly dispersed in 3 mL THC solutions (40 mg L^{-1}), where the pH value of the solution was set as 7.4. The adsorption and measurement processes were consistent with the previous experiment. Finally, 20 mg PMIPs or MIPs was evenly dispersed in 3 mL THC solutions (40 mg L^{-1}, pH = 7.4). After stirring at different temperatures (25–65 °C) for 24 h, the residual amount of THC was measured by a UV–vis spectrophotometer.

Study on drug release behavior

The dialysis method was used to evaluate the drug release abilities of the four adsorbents. The specific processes were as follows: 20 mg adsorbent loaded THC was evenly dispersed in deionized water and then placed into a dialysis bag with a molecular interception weight of 2000. Then, the dialysis bag was immersed in a phosphate buffer and incubated in a constant temperature shaker. Different temperatures (25 or 37 °C) and buffer pH (1.7 or 7.4) were investigated, respectively. At the predetermined time, 3 mL release solution was collected, and added the same volume of fresh buffer solution to the system. The amount of THC in the release solution was measured by a UV–vis spectrophotometer.

Results and discussion

Synthesis of degradable hyperbranched polymers

The first step in preparing PMIPs is synthesizing cleavable double bond hyperbranched polymers by the Michael addition [3 + 2] of A_2 and B_3 monomers. The A_2 monomer was synthesized by esterification reaction of bis(2-hydroxyethyl) disulfide and acryloyl chloride, which aimed to introduce the disulfide bonds linker and the double bond groups. The chemical structure of the A_2 monomer was characterized by ^{1}H-NMR (Fig. S1A) and FT-IR (Fig. S1B). The signal peaks at δ_H 6.34 (a), δ_H 6.08 (b), and δ_H 5.79 (c) ppm corresponded to –CH=CH_2 protons of acryloyl chloride, and δ_H 4.35 (d) and δ_H 2.89 (e) corresponded to the characteristic peaks of protons in –CH_2–, which was consistent with the structure of A_2 monomer. In addition, the FTIR spectrum was used to verify the functional groups of the A_2 monomer. Compared to the reactant bis(2-hydroxyethyl) disulfide (Fig. S1 Ba), the disappeared peak at 3100–3500 cm^{-1} was assigned to the absorption peak of –OH of bis(2-hydroxyethyl) disulfide, and the appearance peaks of 3434, 1727, and 1635 cm^{-1} were assigned to the absorption peak of–CO–O–, the stretch and vibration peak of –C=O, and the absorption peak of –CH=CH_2 of A_2 monomer (in Fig. S1 Bb), respectively. The above results demonstrated the successful synthesis of the A_2 monomer [31].

Secondly, HBP-AP with disulfide bond and terminal double bond was synthesized by the Michael addition reaction of the A_2 and B_3 monomer, where the molar ratio of A_2 and B_3 monomer was 2.2–1.0. Four hyperbranched polymers were synthesized at monomer concentrations of 0.4, 0.8, 1.2, and 1.6 moL L^{-1}, respectively, and GPC with M_n measured their molecular weights and distributions ranged from 1896 to 36,150 g moL^{-1}, and PDI ranged from 1.12 to 4.56 (Table S1). The element composition of HBP-AP was characterized by XPS (Fig. S2A). HBP-AP was mainly composed of C, O, N, and S elements, the contents of which were 74.7%, 24.2%, 0.9%, and 0.2%, respectively. The disulfide bond in HBP-AP can occur in mercapto-disulfide bond exchange reactions in the presence of DTT to dissociate and degrade the polymers (Fig. S2B), and the experimental results showed that HBP-AP was degraded entirely within 10 h in the presence of 4 times DTT, leading a fast degradation rate (Fig. S3).

Preparation of PMIPs

As shown in Fig. 1, we described a novel strategy for PMIPs, the polymerization of functional monomer and cross-linker using HBP-AP as a matrix where hyperbranched polymers with redox stimulus response were synthesized and introduced into the preparation of PMIPs to improve adsorption

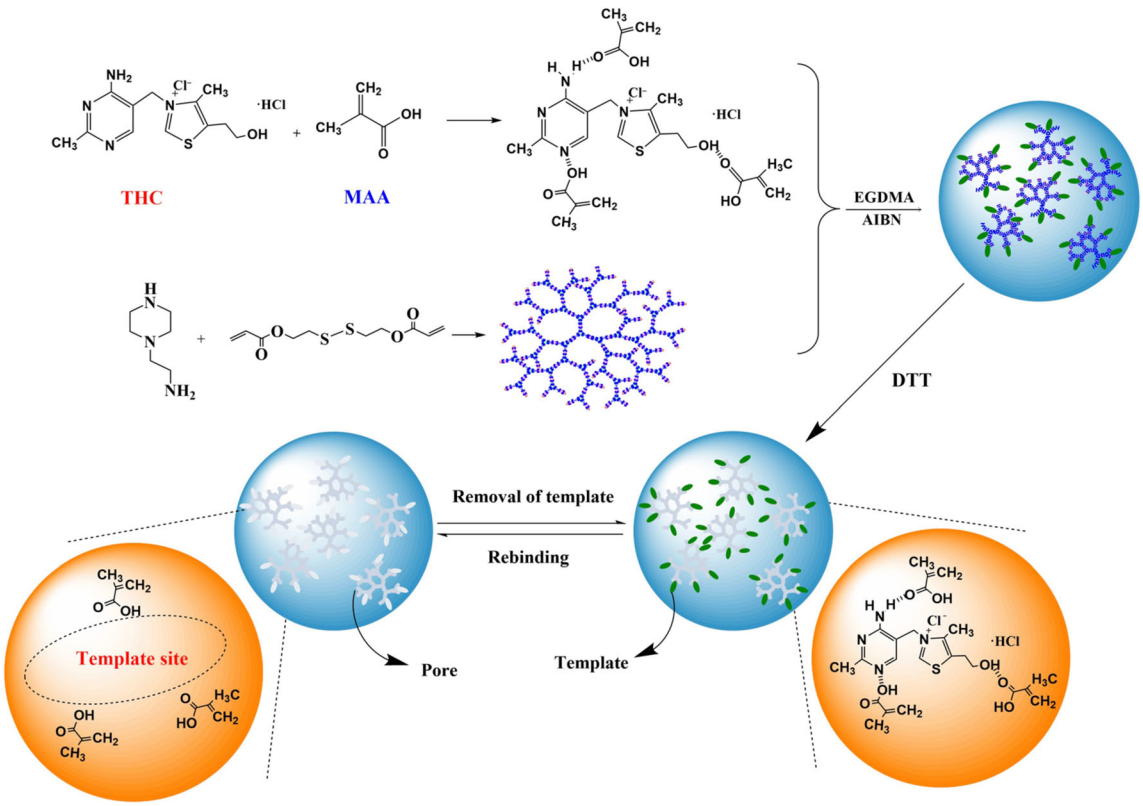

Figure 1 Schematic illustration of the preparation of PMIPs.

performance. Firstly, the effect of molecular weight of HBP-AP on the imprinting effect was investigated.

As shown in Fig. 2a, HBP-AP-2 with a molecular weight of 11,450 g moL^{-1} had the best imprinting effect. The reason was that utilized the reduction and fracture characteristics of reversible disulfide bonds in HBP-AP to form porous channels in MIPs, which expose more effective identification sites and improve adsorption performance. The HBP-AP with low molecular weight had a small proportion of disulfide bonds, resulting in the relatively low adsorption capacity of PMIPs. However, the HBP-AP with high molecular weight led to a high degree of chain entanglement between molecular chains, which hindered the formation of imprinted channels, thus reducing the adsorption capacity of the material. Hence, during the preparation of HBP-AP, the concertation of monomer at 0.8 moL L^{-1}was selected.

Secondly, the mass of HBP-AP used as a matrix was investigated. As depicted in Fig. 2b, when 100 mg HBP-AP was added, the adsorption capacity of PMIPs was the best. However, as the amount of HBP-AP increased, the adsorption capacity decreased. It can infer that when the amount of HBP-AP was more than 100 mg, it was more likely to cause chain entanglement in the system, which will hinder molecular channels, thereby affecting the adsorption capacity of MIPs. Therefore, 100 mg HBP-AP was added in the preparation of PMIPs.

Finally, we also investigated the volume of the solvent. The PMIPs should be prepared in a suitable solvent so that the HBP-AP and functional monomer form a homogeneous solution to get good molecular recognition. Acetonitrile is one of the typical solvents used for imprinting small molecules, and considering the solubility of HBP-AP, the mixture of water and acetonitrile (1:4, v/v) was selected as the solvent. Too much volume of solvent can affect the growth of PMIPs, resulting in incomplete imprinted sites. At the same time, the too low volume of solvent can cause aggregation of PMIPs, and affect the reliability and stability of imprinted sites. According to the experimental results, PMIPs prepared in the mixture of 2.4 mL water and 9.6 mL acetonitrile had the best adsorption capacity (Fig. 2c).

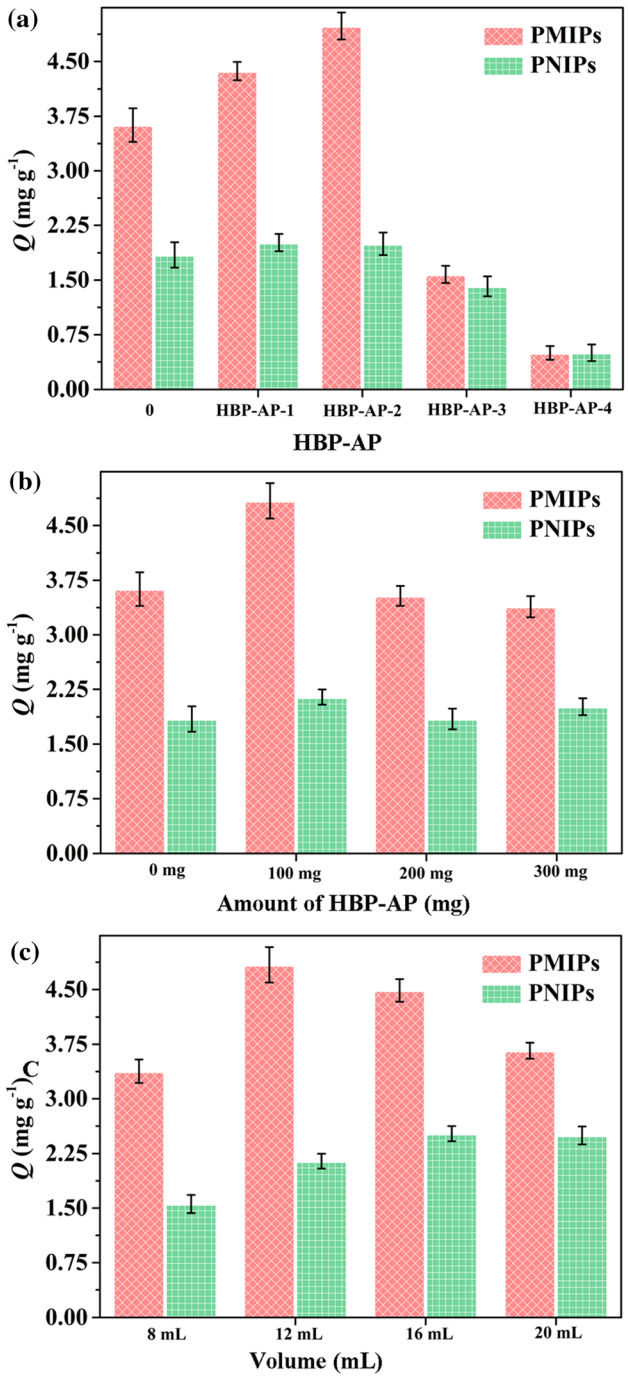

Figure 2 **a** Effects of hyperbranched polymers with different molecular weights on THC adsorption of the obtained materials; **b** Effects of hyperbranched polymers with the different mass on THC adsorption of the obtained materials; **c** Effects of the volume of the reaction solution on THC adsorption of the obtained materials.

Characterization of PMIPs

The morphology of materials was observed by SEM. The cavitation structures of PMIPs (Fig. 3a) and MIPs (Fig. 3c) were more than those of PNIPs (Fig. 3b) and NIPs (Fig. 3d), respectively, which demonstrated that the template molecule has an influence on the formation of microstructure in the process of synthesis. Moreover, compared to the MIPs (Fig. 3c), the regularity and average of PMIPs decreased, and the cavitation content of PMIPs increased (Fig. 3a) because of the degradation of the additional HMP-AR. The above results indicated the successful preparation of imprinted materials containing hyperbranched polymers with degradable disulfide bonds.

The degradation of the disulfide bonds in PMIPs was characterized by XPS. Before degradation, PMIPs were mainly composed of C, O, N, and S elements, whose contents were 75.6%, 23.3%, 0.7%, and 0.4%, respectively (Fig. S4a). After washing with DTT, the HBP-AP in PMIPs was dissociated, N and S elements disappeared, and the remaining C and O contents were 75.7% and 24.3%, respectively (Fig. S4b). The above results showed that the hyperbranched polymers were introduced into imprinted materials, where the disulfide bonds were successfully degraded by DDT washing.

To study the microstructure of materials, the porosity of the four obtained materials was characterized by nitrogen adsorption–desorption isotherms. For PMIPs (Fig. S5A), PNIPs (Fig. S5B), and MIPs (Fig. S5C), when P/P_o was lower than 0.4, the adsorption capacities increased slightly, which indicated a typical I type adsorption characteristic of microporous materials. At this stage, it was observed that multilayer adsorption of nitrogen molecules occurs inside the material. Then, the adsorption capacities changed little in the range of P/P_o of 0.4 to 0.8, which indicated that the mesoporous existed in the materials and capillary condensation of nitrogen molecules occurred in mesoporous part of the materials. These results demonstrated that the mesoporous existed in the above three materials derived from the imprinting process or the cleavage of disulfide bonds in hyperbranched polymers. For NIPs (Fig. S5D), the adsorption capacity decreased rapidly when P/P_o was below 0.8. When P/P_o exceeded 0.8, the adsorption capacity increased substantially, which came from the adsorption of material, demonstrating that no mesoporous existed in

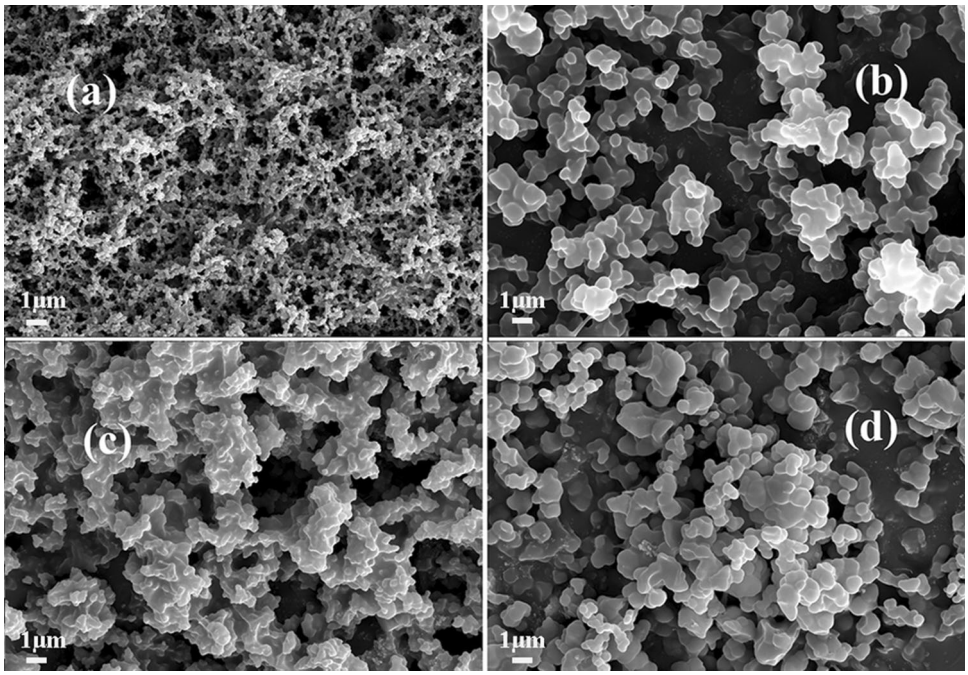

Figure 3 SEM images of PMIPs (**a**), PNIPs (**b**), MIPs (**c**), and NIPs (**d**).

Table 1 The data of nitrogen adsorption–desorption isotherms

	Total pore volume ($cm^3\ g^{-1}$)	Micro pore volume ($cm^3\ g^{-1}$)	Pore size distribution (nm)	Specific surface area ($m^2\ g^{-1}$)
PMIPs	0.0428	0.0032	4.64	33.23
MIPs	0.0134	0.0035	7.91	16.04
PNIPs	0.0059	0.0030	10.53	4.31
NIPs	0.0019	0.0029	83.82	2.91

NIPs. In addition, as listed in Table 1, PMIPs had the highest total pore volume (0.0428 $cm^3\ g^{-1}$) and specific surface area (33.23 $m^2\ g^{-1}$), indicating that more mesoporous existed in PMIPs than MIPs, derived from the cleavage of disulfide bonds in hyperbranched polymers, which was conducive to the mass transfer of adsorbents.

Analysis of adsorption isotherms

The adsorption isotherms of THC to PMIPs, PNIPs, MIPs, and NIPs at concentrations of 20–1200 mg L^{-1} were assessed and shown in Fig. 4a. For the presence of imprinting sites in MIPs, both PMIPs (101.25 mg g^{-1}) and MIPs (39.86 mg g^{-1}) showed better adsorption capacity for THC than PNIPs (16.57 mg g^{-1}) and NIPs (10.92 mg g^{-1}). Moreover, the adsorption capacity of PMIPs was more than that of MIPs, which proves that the porous channels of PMIPs from the cleavage of disulfide bonds in hyperbranched polymers can increase the chance and probability of THC entering into the imprinted sites inside the materials, thereby improving the adsorption capacity of PMIPs.

The equilibrium data were further analyzed using the Freundlich and Langmuir isothermal model to analyze the affinity distribution (Fig. 4b and Fig. S6). By comparing the values of correlation coefficient (r) in Table 2, the Freundlich isothermal model is found to fit better the binding data of THC on PMIPs and MIPs, and the values of r were 0.9923 and 0.9324, respectively. These results demonstrated that the adsorption process of imprinted materials to THC conformed to a multilayer adsorption heterogeneous system [32]. The amounts of THC bound to PMIPs and MIPs increased along with its initial concentration, and the amount of THC attached to the PMIPs is the highest (Fig. 4b). The results illustrated the specific binding of PMIPs with template and the success of the imprinting process. The better

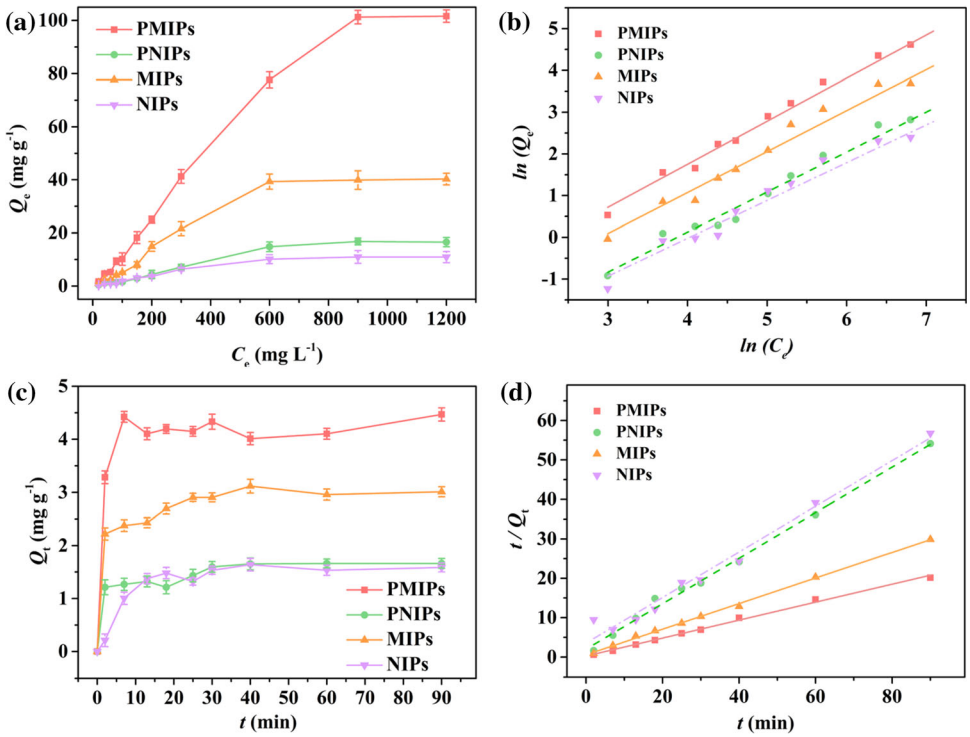

Figure 4 **a** Adsorption isotherms; **b** The adsorption isotherm experiments data were fitted by the Freundlich isothermal model; **c** Adsorption kinetics; **d** The experimental kinetic data were fitted by the pseudo-second-order kinetic model.

Table 2 Freundlich and Langmuir fitting parameters for the prepared materials

Isotherm	Parameter	Materials			
		PMIPs	PNIPs	MIPs	NIPs
Freundlich	K_F ((mg/g)·(L/mg)$^{-1}$)	16.1013	56.4299	32.5867	68.7927
	$1/n$	1.1261	1.0342	1.1291	1.0427
	R^2	0.9915	0.9718	0.9843	0.9750
Langmuir	R^2	0.2236	0.7242	0.6281	0.3193

adsorption ability of PMIPs is attributed to the porous structure and the cleavage of disulfide bonds in hyperbranched polymers [33]. The above results indicated the porous structure formed in PMIPs facilitated the mass transfer and increased the adsorption capacity.

Analysis of adsorption kinetics

The adsorption kinetics of THC to PMIPs, PNIPs, MIPs, and NIPs were assessed at 0–90 min. As Fig. 4c illustrated, the adsorption amount of THC increased significantly in the first 10 min and then reached the adsorption equilibrium for PMIPs, which is a shorter adsorption time than MIPs. These results showed that the adsorption sites of PMIPs can be quickly occupied by template molecules, exhibiting fast mass transfer. Moreover, the adsorption capacity of PMIPs was higher than those of the other three materials. This was due to the formation of porous channels in PMIPs, which was conducive to the rapid interaction between adsorbents and imprinted sites, thus improving the adsorption capacity.

Furthermore, adsorption kinetics data are fitted by the pseudo-first-order and pseudo-second-order kinetic models (Fig. 4d and Fig S7). The results are depicted in Table 3. The pseudo-second-order kinetic model can better reflect the kinetic adsorption process of the four materials to THC because of the high values of r (0.9821–0.9987). Moreover, the fitted $Q_{e,\mathrm{cal}}$ (1.73–4.39 mg g^{-1}) was closer to the experimental data $Q_{e,\mathrm{exp}}$ (1.64–4.47 mg g^{-1}). The discussion indicated that the adsorption rate was determined by the concentration of adsorbents in solution and the number of adsorption sites of the obtained materials,

Table 3 Pseudo-first-order and pseudo-second-order kinetic models fitting parameters of four materials

Materials	$Q_{e,exp}$	2nd-order kinetic model			1st-order kinetic model		
		$t/Q_t = 1/(K_2Q_e^2) + t/Q_e$			$\log(Q_e - Q_t) = \log(Q_e) - (k_1/2.303)t$		
		$Q_{e,cal}$ (mg/g)	$K_2(\times 10^4)$ (g/(mg min)	R^2	$Q_{e,cal}$ (mg/g)	$K_2(\times 10^4)$ (g/(mg min)	R^2
PMIPs	4.47	4.39	0.228	0.9959	0.51	0.012	0.1307
PNIPs	1.66	1.73	0.577	0.9948	3.33	0.004	0.8253
MIPs	3.12	3.08	0.325	0.9987	1.15	0.082	0.9161
NIPs	1.64	1.73	0.578	0.9821	1.11	0.077	0.7487

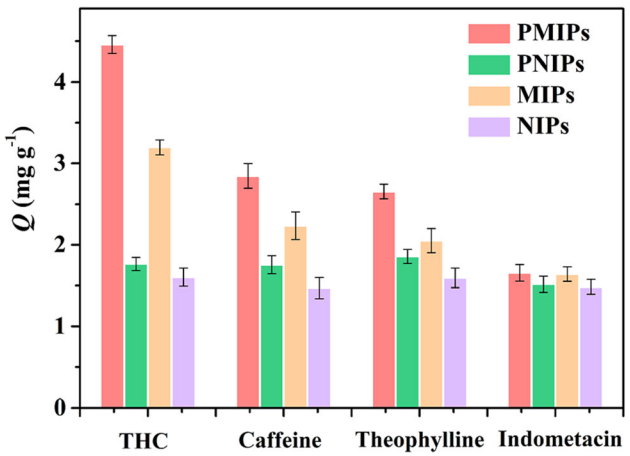

Figure 5 Specific selectivity of the obtained materials for THC, caffeine, theophylline, and indomethacin.

which was controlled by the chemical adsorption mechanism [34, 35].

Analysis of selective adsorption

TO investigate the specific selectivity of imprinted materials to THC, three other compounds, including theophylline, caffeine, and indomethacin, were selected as the references, and the adsorption capacities were presented in Fig. 5. The adsorption capacities of PMIPs (4.45 mg g^{-1}) and MIPs (3.19 mg g^{-1}) to THC were higher than those of PNIPs (1.76 mg g^{-1}) and NIPs (1.60 mg g^{-1}). This was because the imprinted sites formed in PMIPs and MIPs had a size and structure matching THC, producing a strong affinity, showing the specific selective adsorption to THC. For PMIPs, the porous structure was conducive to THC adsorption, resulting in higher adsorption capacity than MIPs. Moreover, the four materials showed similar adsorption behaviors to theophylline and caffeine because of the similar chemical structure to THC. In comparison, the imprinted materials showed similar and low adsorption capacities to non-imprinted materials to indomethacin (1.48–1.65 mg g^{-1}). The reason was that the structure of indomethacin was significantly different from THC, which was not enough to fully match the imprinted sites of THC, resulting in weak binding and poor affinity. It indicated that PMIPs had an excellent selectivity to THC and poor adsorption ability to the compounds with noticeable structural differences [36, 37].

Drug loading influences factors

The pH value of the solution was an essential factor affecting the binding of THC to the imprinting material. Therefore, adsorption experiments were performed at different pH values ranging from 1.7 to 8.0. As shown in Fig. 6a, for PMIPs and MIPs, when the pH value was below 5, the adsorption capacities were deficient. After that, with the rise in pH value, the adsorption capacities significantly increased, reached the maximum at pH 7.4, and began declining. It was because the acidic environment would destroy the hydrogen bond between the imprinted material and the template molecule. In addition, when the solution was fundamental, protons interacting with the organic surface of imprinted materials were reduced because the pKa of THC was about 4.8. Hence, the adsorption process was conducted at pH 7.4.

The effect of the mass of the adsorbent on adsorption capacity was investigated from 5 to 30 mg. The results in Fig. 6b demonstrated that adsorption capacity also increased with the increase in mass of adsorbents. Moreover, 20 mg of PMIPs was sufficient to obtain the maximum adsorption

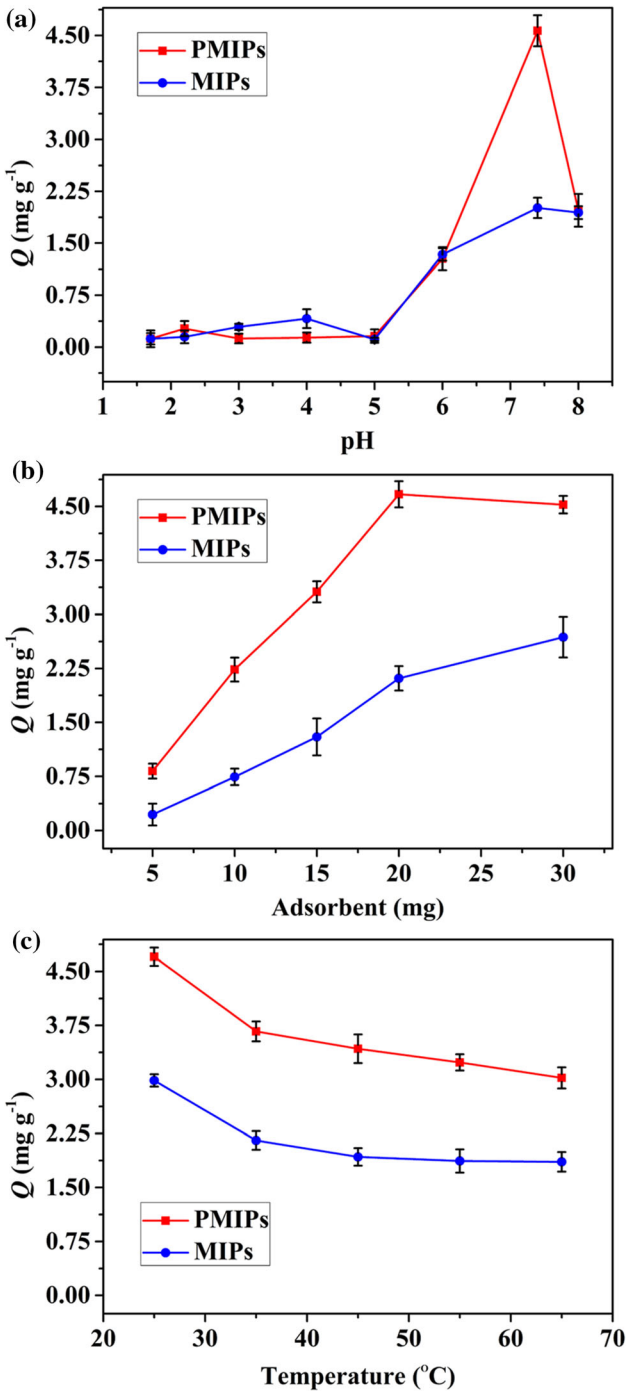

Figure 6 Optimization of **a** pH value of the solution, **b** mass of adsorbent, and **c** temperature for drug loading.

capacity, while 30 mg of MIPs was still insufficient. The results indicated that there were more imprinted sited in PMIPs than those in MIPs, due to the form of porous structure in PMIPs, resulting in more imprinted sites being exposed. Hence, 20 mg of adsorbent was selected for adsorption.

The effect of solution temperature on adsorption capacity was also investigated from 25 to 65 °C. Figure 6c shows that as the temperature increased, the adsorption capacity decreased, and the maximum adsorption capacity appeared at 25 °C. It was because with the increase in temperature, the diffusion rate of solute molecules in solution increased, which was not conducive to the transfer of solute molecules to the adsorption site of imprinted materials. Hence, 25 °C was selected for adsorption.

Drug release behaviors

The factors affecting drug release from imprinted materials were examined, including temperature and pH value of the solution. Firstly, the influence of temperature on drug release was investigated. Figure 7 presents the THC release behaviors at 25 (Fig. 7a) and 37 °C (Fig. 7b). Both PMIPs and MIPs

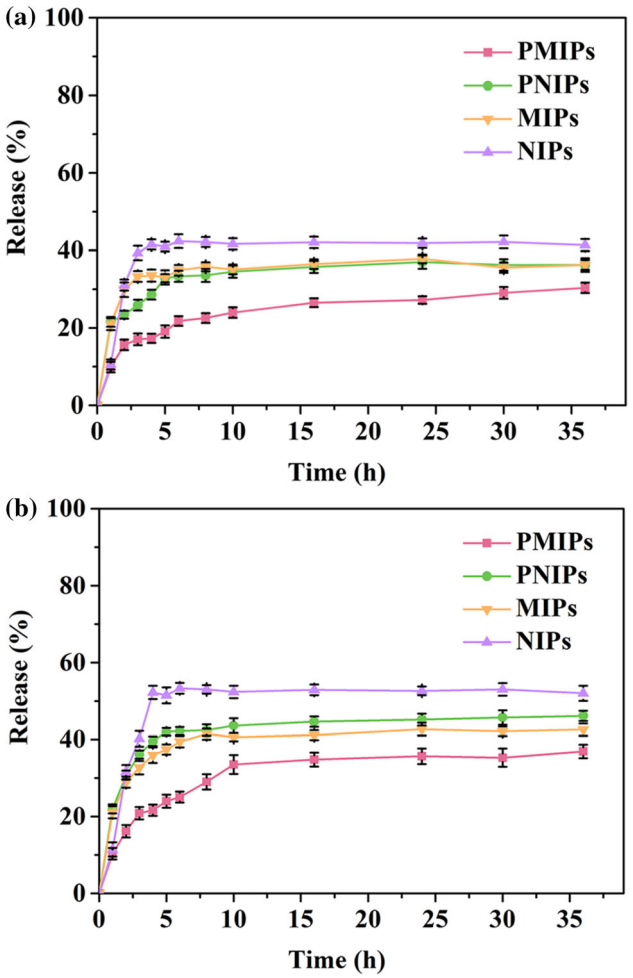

Figure 7 Effect of temperature on drug release. **a** 25 °C; **b** 37 °C.

showed similar slow release behavior at 25 and 37 °C in 2 h and the release rate was unaffected by temperature. After 2 h, a higher release rate of THC was demonstrated when temperature was increased to 37 °C. The results combining drug loading experiments showed that high temperature was not conductive to drug loading but conducive to drug release. This body temperature release characteristic is beneficial for the DDS system. Then different kinetic models such as Zero-order model, First-order model, and Higuchi's model were evaluated from drug release experiments [38]. The value of r^2 for each kinetic model was calculated to determine a more appropriate release model. The values of r^2 (Table S2) showed in larger values for all the materials at 37 °C, and the largest value r^2 for PMIPs, 0.9437, indicated that PMIPs were more in agreement with a Higuchi's model diffusion mechanism and the release depends on the THC diffusion from the polymer matrix. The porous structure introduced by HBP-AP can modify the drug diffusion and a higher temperature was favored to drug release.

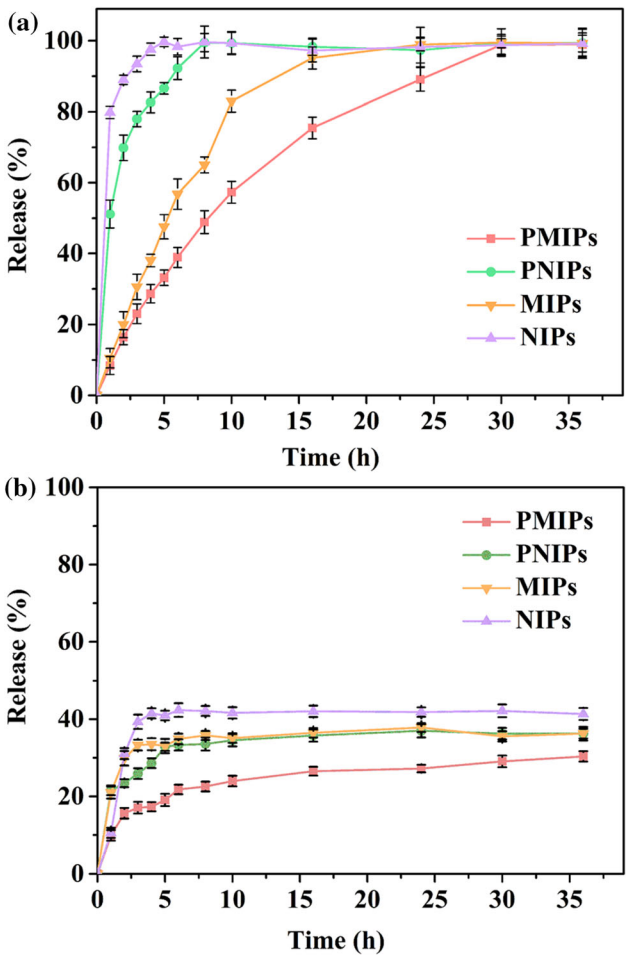

Figure 8 Effect of pH value of the solution on drug release. **a** pH 1.7; **b** pH 7.4.

In addition, the influence of the pH value of the solution on drug release was investigated. Figure 8 presents the THC release behaviors in pH 1.7 and 7.4. In the solution of pH 1.7 (Fig. 8a), PNIPs and NIPs exhibited a fast release rate, and the release was completed within 8 h, while PMIPs and MIPs required 32 and 16 h to achieve the full release of THC, respectively. In the solution of pH 7.4 (Fig. 8b), all four adsorbents showed similar release behavior. Their release rates were not high (25–40%), which can be achieved in less than 5 h. The three diffusion kinetic models were also evaluated from the data obtained during the drug release experiments to determine the value of r^2. The PMIPs resulted in the largest value of r^2 at pH 1.7 for Higuchi's model (Table S3). For example, the value of r^2 was equal to 0.9945 and 0.8920 at pH 1.7 and pH 7.4, respectively, while for the control PNIPs, MIPs and NIPs system, the r^2 value was 0.7927, 0.9825, and 0.5171 at pH 1.7 for Higuchi's model, respectively. The correlation coefficient increased as the pH of the release medium was more acidic. Furthermore, both the imprinted matrix had better correlation coefficient than non-imprinted matrix no matter at release pH 1.7 or 7.4. All the above results indicated that the imprinted sites of PMIPs and MIPs bound with THC through hydrogen bonds and released slowly. The form of porous structure in PMIPs allowed more THC to bind with imprinted sites, and the imprinted networks did play the exact role to modify drug diffusion at two different pH values, resulting in a longer release time. Moreover, THC can be released slowly under acidic conditions but are not conducive to release under neutral conditions.

Conclusions

In a word, we have successfully developed porous designed MIPs based on sensitive cleavage bonds for drug-controlled release. The hyperbranched polymer with a terminal double bond and sensitive disulfide bond was synthesized, which was then introduced into the preparation of MIPs as the matrix. Compared with traditional molecularly imprinted materials, the obtained MIPs were porous, producing more imprinted adsorption sites and faster mass transfer.

Moreover, the obtained porous MIPs exhibited better drug loading capacity and sustained release behavior, which showed great potential as drug delivery carriers. In summary, our porous design strategy improved and diversified the structure and function of MIPs. This platform approach also provided an alternative solution for the rational design of an improved drug delivery system.

Acknowledgements

This work was supported by the Natural Science Foundation of Shaanxi Province (No. 2017JQ2004).

Declarations

Conflict of interest The authors declare that they have no known competing financial interests or personal relationships that could have appeared to influence the work reported in this paper.

Supplementary Information: The online version contains supplementary material available at https://doi.org/10.1007/s10853-022-08049-z.

References

[1] Song G, Cheng L, Chao Y, Yang K, Liu Z (2017) Emerging nanotechnology and advanced materials for cancer radiation therapy. Adv Mater 29:1700996

[2] Chen Y, Fan ZX, Zhang ZC, Niu WX, Li CL, Yang NL, Chen B, Zhang H (2018) Two-dimensional metal nanomaterials: synthesis, properties, and applications. Chem Rev 118:6409–6455

[3] Nuria RV, Stephan S, Luis FS, Manuel A, Juan RG (2013) Synthesis of cyclic γ-amino acids for foldamers and peptide nanotubes. Eur J Org Chem 2013:3477–3493

[4] Ramasamy T, Ruttala HB, Gupta B, Poudel BK, Choi HG, Yong CS, Kim JO (2017) Smart chemistry-based nanosized drug delivery systems for systemic applications: a comprehensive review. J Control Release 258:226–253

[5] Hu Q, Bu YS, Zhen XY, Xu K, Ke RF, Xie XY, Wang SC (2019) Magnetic carbon nanotubes camouflaged with cell membrane as a drug discovery platform for selective extraction of bioactive compounds from natural products. Chem Eng J 364:269–279

[6] Bourquin J, Milosevic A, Hauser D, Lehner R, Blank F, Petri-Fink A, Rothen-Rutishauser B (2018) Biodistribution, clearance, and long-term fate of clinically relevant nanomaterials. Adv Mater 30:1704307

[7] Gai SL, Yang GX, Yang PP, He F, Lin J, Jin DY, Xing BG (2018) Recent advances in functional nanomaterials for light-triggered cancer therapy. Nano Today 19:146–187

[8] Nerantzaki M, Michel A, Petit L, Garnier M, Menager C, Griffete N (2022) Biotinylated magnetic molecularly imprinted polymer nanoparticles for cancer cell targeting and controlled drug delivery. Chem Commun 58:5642–5645

[9] Lu HF, Xu SX, Guo ZC, Zhao MH, Liu Z (2021) Redox-responsive molecularly imprinted nanoparticles for targeted intracellular delivery of protein toward cancer therapy. ACS Nano 15:18214–18225

[10] Chen FF, Wang JY, Chen HR, Lu RC, Xie XY (2018) Microwave-assisted RAFT polymerization of well-constructed magnetic surface molecularly imprinted polymers for specific recognition of benzimidazole residues. Appl Surf Sci 435:247–255

[11] Corman ME, Cetinkaya A, Ozcelikay G, Ozgur E, Atici EB, Uzun L, Ozkan SA (2021) A porous molecularly imprinted nanofilm for selective and sensitive sensing of an anticancer drug ruxolitinib. Anal Chim Acta 1187:339143

[12] Tuwahatu CA, Yeung CC, Lam YW, Roy VAL (2018) The molecularly imprinted polymer essentials: curation of anticancer, ophthalmic, and projected gene therapy drug delivery systems. J Control Release 287:24–34

[13] Hua YB, Kukkar D, Brown RJC, Kim KH (2022) Recent advances in the synthesis of and sensing applications for metal-organic framework-molecularly imprinted polymer (MOF-MIP) composites. Crit Rev Environ Sci Technol. https://doi.org/10.1080/10643389.2022.2050161

[14] BelBruno JJ (2019) Molecularly imprinted polymers. Chem Rev 119:94–119

[15] Haupt K, Rangel PXM, Tse Sum Bui B (2020) Molecularly imprinted polymers: antibody mimics for bioimaging and therapy. Chem Rev 120:9554–9582

[16] Janczura M, Luliński P, Sobiech M (2021) Imprinting technology for effective sorbent fabrication: current state-of-art and future prospects. Materials 14:1850

[17] Song ZH, Li JH, Lu WH, Li BW, Yang GQ, Bi Y, Arabi M, Wang XY, Ma JP, Chen LX (2022) Molecularly imprinted polymers based materials and their applications in chromatographic and electrophoretic separations. TrAC Trend Anal Chem 146:116504

[18] Liu R, Poma A (2021) Advances in molecularly imprinted polymers as drug delivery systems. Molecules 26:3589

[19] Torabi SJ, Mohebali A, Abdouss M, Shakiba M, Abdouss H, Ramakrishna S, Teo YS, Jafari I, Ghomi ER (2021) Synthesis and characterization of a novel molecularly imprinted

polymer for the controlled release of rivastigmine tartrate. Mater Sci Eng C Mater Biol Appl 128:112273
[20] Schirhagl R (2014) Bioapplications for molecularly imprinted polymers. Anal Chem 86:250–261
[21] Jia M, Yang J, Zhao YX, Liu ZS, Aisa HA (2017) A strategy of improving the imprinting effect of molecularly imprinted polymer: effect of heterogeneous macromolecule crowding. Talanta 175:488–494
[22] Chen FF, Chen H, Duan X, Jia JQ, Kong J (2016) Molecularly imprinted polymers synthesized using reduction-cleavable hyperbranched polymers for doxorubicin hydrochloride with enhanced loading properties and controlled release. J Mater Sci 51:9367–9383. https://doi.org/10.1007/s10853-016-0183-2
[23] Chen H, Kong J, Tian W, Fan XD (2012) Intramolecular cyclization in $(A_2) + (B_3)$ polymers via step-wise polymerization resulting in a highly branched topology: quantitative determination of cycles by combined NMR and SEC analytics. Macromolecules 45:6185–6195
[24] Schuell C, Frey H (2013) Grafting of hyperbranched polymers: from unusual complex polymer topologies to multivalent surface functionalization. Polymer 54:5443–5455
[25] Smeets NMB (2013) Amphiphilic hyperbranched polymers from the copolymerization of a vinyl and divinyl monomer: the potential of catalytic chain transfer polymerization. Eur Polym J 49:2528–2544
[26] Guo M, Wang R, Jin ZC, Zhang XY, Jokerst JV, Sun YT, Sun LP (2022) Hyperbranched molecularly imprinted photoactive polymers and its detection of tetracycline antibiotics. ACS Appl Polym Mater 4:1234–1242
[27] Kaur K, Jindal R, Jindal D (2020) Controlled release of vitamin B-1 and evaluation of biodegradation studies of chitosan and gelatin based hydrogels. Int J Biol Macromol 146:987–999
[28] Fathima SJ, Fathima I, Abhishek V, Khanum F (2016) Phosphatidylcholine, an edible carrier for nanoencapsulation of unstable thiamine. Food Chem 197:562–570
[29] Allahkarami E, Dehghan Monfared A, Silva LFO, Dotto GL (2022) Lead ferrite-activated carbon magnetic composite for efficient removal of phenol from aqueous solutions: synthesis, characterization, and adsorption studies. Sci Rep 12:10718
[30] Franco DSP, Pinto D, Georgin J, Netto MS, Foletto EL, Manera C, Godinho M, Silva LFO, Dotto GL (2022) Conversion of *Erythrina speciosa* pods to porous adsorbent for Ibuprofen removal. J Environ Chem Eng 10:108070
[31] Hong CY, You YZ, Wu DC, Liu Y, Pan CY (2007) Thermal control over the topology of cleavable polymers: from linear to hyperbranched structures. J Am Chem Soc 129:5354–5355
[32] Bu YS, Hu Q, Zhang XL, Li T, Xie XY, Wang SC (2020) A novel cell membrane-cloaked magnetic nanogripper with enhanced stability for drug discovery. Biomater Sci 8:673–681
[33] Chen FF, Wang JY, Lu RC, Chen HR, Xie XY (2018) Fast and high-efficiency magnetic surface imprinting based on microwave-accelerated reversible addition fragmentation chain transfer polymerization for the selective extraction of estrogen residues in milk. J Chromatogr A 1562:19–26
[34] Hu Q, Bu YS, Cao RQ, Zhang G, Xie XY, Wang SC (2019) Stability designs of cell membrane cloaked magnetic carbon nanotubes for improved life span in screening drug leads. Anal Chem 91:13062–13070
[35] Xie XY, Hu Q, Ke RF, Zhen XY, Bu YS, Wang SC (2019) Facile preparation of photonic and magnetic dual responsive protein imprinted nanomaterial for specific recognition of bovine hemoglobin. Chem Eng J 371:130–137
[36] Chen FF, Mao M, Wang JY, Liu JW, Li F (2020) A dual-step immobilization/imprinting approach to prepare magnetic molecular imprinted polymers for selective removal of human serum albumin. Talanta 209:120509
[37] Hao Y, Gao RX, Liu DC, Tang YH, Guo ZJ (2015) Selective extraction of gallic acid in pomegranate rind using surface imprinting polymers over magnetic carbon nanotubes. Anal Bioanal Chem 407:7681–7690
[38] Ruela ALM, Figueiredo EC, Pereira GR (2014) Molecularly imprinted polymers as nicotine transdermal delivery systems. Chem Eng J 248:1–8